

INDUCTANCE MODELING FOR ON-CHIP INTERCONNECTS

Shang-Wei Tu*, **Wen-Zen Shen**, **Yao-Wen Chang****, **Tai-Chen Chen****, and
Jing-Yang Jou*

*Department of Electronics Engineering, National Chiao Tung University, Hsinchu, Taiwan ROC

**Graduate Institute of Electronics Engineering & Department of Electrical Engineering, National Taiwan University, Taipei, Taiwan ROC

Abstract *As the operation frequency reaches gigahertz in deep-submicron designs, the effects of inductance on noise and delay can no longer be neglected. Most of the previous works on inductance extraction are field-solvers, which are intrinsically more accurate but computationally expensive. Others focus on modeling the inductances of special routing topologies such as the bus structure. Therefore, it is not suitable to incorporate them on-line into a layout (placement and routing) tool for inductance (delay and noise) optimization. In this paper, we consider the overlapping of unequal wire lengths and dimensions to efficiently extract the loop inductance from the coplanar interconnect structure. The difference between our simulation results and the estimation values obtained by FastHenry [11] is within 10% for practical cases. In particular, our modeling is extremely efficient, and thus can be incorporated into a layout tool for inductance optimization.*

1. Introduction

As technology advances into the very deep-submicron era, interconnection delay dominates overall circuit performance and noise becomes more serious than before. Therefore, accurately predicting the interconnection delay and noise becomes a major challenge in high performance designs. For deep-submicron, high-performance circuits, ignoring inductance effects may incur a large amount of error, since an RC model as compared to an RLC model may create errors of up to 30% in the total propagation delay of a repeater system [10], and in some worst cases the noise coupling due to C and L may reach around 55% of the supply voltage [8]. As technology improves and die size increases, short rise/fall times of signals and long wires make inductance effects much more significant than before [14]. Therefore, it is very important to consider the self and coupling inductance.

Inductance extraction has been studied extensively in the literature. Grover [7] collected many formulas for extracting inductance. However, as mentioned in [9], there are limitations of applying the equations. For example, they do not consider internal inductance, and wire widths are not considered for mutual inductance. Also, Qi et al. [13] proposed some formulas for extracting bus structure's inductance with considering different effects such as skin effect and substrate effect. Greengard developed a multipole method to extract inductances [6]. Phillips, Kamon, and White [12] proposed an FFT-based approach for 3-D inductance extraction. Beattie and Pileggi proposed a hierarchical refinement method [3] that improves the running time for capturing the near field effects. Also, Beattie et al. proposed equipotential shells methodology [2] to efficiently extract the inductance of the bus structure. He et al. presented a table-based approach to identify the structure of a circuit for inductance extraction [9].

Most of the previous works are field-solvers that are intrinsically more accurate but are computationally expensive. Others focus on modeling the inductances of special routing topologies such as the bus structure. Therefore, it is not suitable to incorporate them on-line into a layout tool for inductance optimization. As [4] pointed out, no good approximation formula exists for coupling inductances of two parallel lines of unequal lengths and dimensions. We consider the overlapping of unequal wire lengths and dimensions (widths and heights) to extract the self and coupling inductance. We derive formulae and models to approximate both self and coupling inductance efficiently yet accurately for the coplanar routing structure. Simulation results show that the difference of the inductance values extracted from our models for practical cases is within 10% for the wires of unequal lengths and dimensions, compared with FastHenry [11]. In particular, our method is extremely fast. For example, the running time for extracting the coupling inductance of two wires of 2000 μm by using our analytical formulas is typically within 0.11 seconds using Mathematica on a 566 MHz Celeron PC with 128 MB RAM while FastHenry requires 141 seconds on SUN Sparc Ultra 60 with dual CPUs and 2GB memory. Therefore, it is feasible to incorporate our model into a layout tool on-line.

The rest of this paper is organized as follows. Section 2 describes the coplanar interconnect structure and some basic electromagnetic concepts. Section 3 derives formulae for self and coupling inductance. Section 4 gives the simulation results on the comparisons between our methods and FastHenry. Finally, Section 5 concludes our work.

2. Preliminaries

In this section, we describe some basic concepts of electromagnetism [5]. We first describe inductance in Subsection 2.1, and then introduce the coplanar structure used in this paper in Subsection 2.2.

2.1 Inductance

Considering two neighboring closed loops, C_1 and C_2 bounding surface S_1 and S_2 , respectively, as shown in Figure 1. If a current I_1 flows in C_1 , a magnetic field \vec{B}_1 will be created. Some of the magnetic flux due to \vec{B}_1 will link with C_2 —that is, it will pass through the surface S_2 bounded by C_2 . We refer to this mutual flux as Φ_{12} . We have

$$\Phi_{12} = \int_{S_2} \vec{B}_1 \cdot d\vec{s}_2 . \quad (1)$$

From *Faraday's law* of electromagnetic induction, we know that a time-varying I_1 (and therefore a time-varying Φ_{12}) will produce an induced electromotive force or voltage in C_2 . However, Φ_{12} exists even if I_1 is a steady d-c current. From *Ampère's circuital law* [5] (Equation 2)

$$\oint_C \vec{B} \cdot d\vec{l} = \mu_0 I , \quad (2)$$

we know that B_1 is directly proportional to I_1 ; hence Φ_{12} is also proportional to I_1 . We have

$$\Phi_{12} = L_{12} I_1 , \quad (3)$$

where the proportionality constant L_{12} is called the mutual inductance or coupling inductance between loops C_1 and C_2 , with SI unit henry (H). In case C_2 has N_2 turns, the flux linkage Λ_{12} due to Φ_{12} is

$$\Lambda_{12} = N_2 \Phi_{12} , \quad (4)$$

Combining Equations (3) and (4), we have

$$L_{12} = \frac{\Lambda_{12}}{I_1} . \quad (5)$$

The coupling inductance between two circuits is then the magnetic flux linkage with the victim circuit (C_2 in Figure 1) per unit current in the aggressor circuit (C_1 in Figure 1).

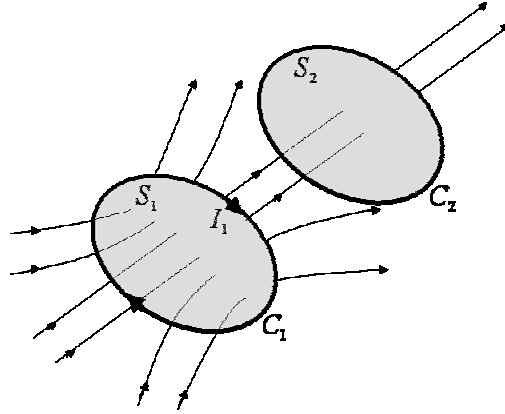


Figure 1: Two magnetically coupled loops.

Some of the magnetic flux produced by I_1 links only with C_1 itself, but not with C_2 . The total flux linkage with C_1 caused by I_1 is

$$\Lambda_{11} = N_1 \Phi_{11}. \quad (6)$$

The self-inductance of loop C_1 is defined as the magnetic flux linkage per unit current in the loop itself; that is

$$L_{11} = \frac{\Lambda_{11}}{I_1}. \quad (7)$$

2.2 Coplanar Structure

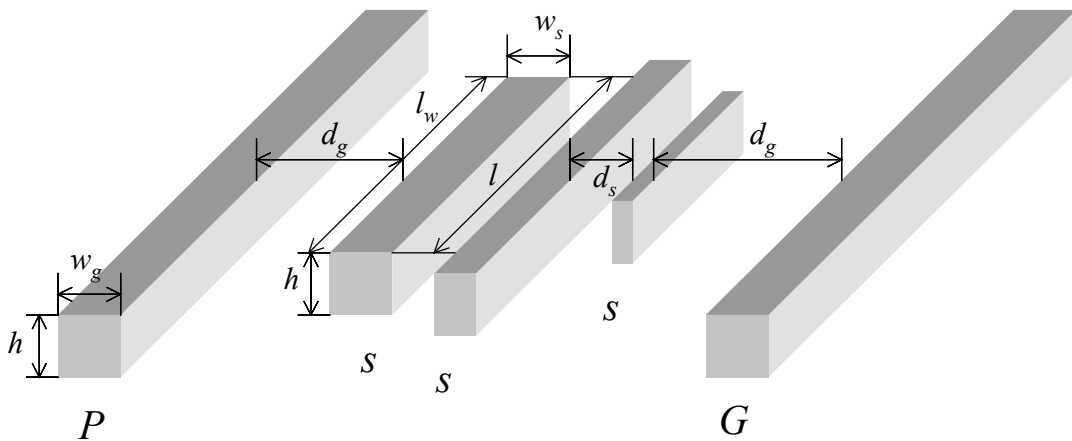


Figure 2: Coplanar interconnect structure.

In this subsection, we introduce the coplanar interconnect structure and the notation which is intensively used in this paper. Figure 2 depicts the coplanar interconnect structure. Here, s stands for a signal wire while P and G stands for a power and a ground grid of identical width, w_g . Throughout this paper, both P and G are considered as ground wires. Assume that all wires are of the same height h , the width and length of each signal wire are w_s and l_w respectively, and the overlapping length of two signal wires is l . We use L_i to represent the self-inductance of s_i and L_{ij} for the coupling inductance between s_i and s_j . Throughout our paper, we assume quasi-static conditions, which imply that the currents vary very slowly in time and the dimensions of circuits are very small in comparison to the wavelength, and set the clock frequency to 3 GHz in our experiments.

Also, we assume that all signals use the nearest P/G wires as their return paths, same as [15]. Although quiet or opposite-switching neighboring nets may also serve as return paths, they are not ideal because currents returning from signal wires have to go through devices, which have significant resistances [15]. Therefore, the other wires that are not involved in the computation for the inductance between wires i and j are assumed floating. From Faraday's law, we know that a floating wire will not affect the inductance computation since it cannot form any current loop.

3. Inductance Modeling

In Subsection 3.1, we derive our formula *AMAS* (Analytical Model Approximation of Self-inductance) for extracting self-inductance in the coplanar structure. Subsection 3.2 *AMAC* (Analytical Model Approximation of Coupling Inductance) is derived for extracting coupling inductance in the coplanar structure. Finally, we re-derive two formulas, *IAMAC* (Improved Analytical Model Approximation of Coupling Inductance) and *IAMAS* (Improved Analytical Model Approximation of Self-inductance), to apply on some corner cases for extracting inductances.

3.1 Self-inductance

Because the rectangular shape of wires, as illustrated in Figure 2, is complex for the computation of the magnetic flux density vector induced from it when carrying current, we apply cylindrical approximation for rectangular conductors. Figure 3 illustrates the approximation. If the current I_i flows in wire s_i and ground wire and its direction is shown as in Figure 3, the current loop C can be determined by the dashed line. The area of S_i , the gray region shown in Figure 3, is determined by the enclosed region of the loop C . To derive self-inductance from Equation (7), we need to compute N_i , S_i , and \vec{B}_i ,

since $\Lambda_i = N_i \Phi_i = N_i \int_{S_i} \vec{B}_i \cdot d\vec{s}_i$. Although $N_i = 1$ and S_i are already known, \vec{B}_i now is still unknown. Hence, we shall first derive the formula of the magnetic flux density vector \vec{B}_i . Note that the unit of L' is henry per meter (H/m) and the unit of L is henry (H).

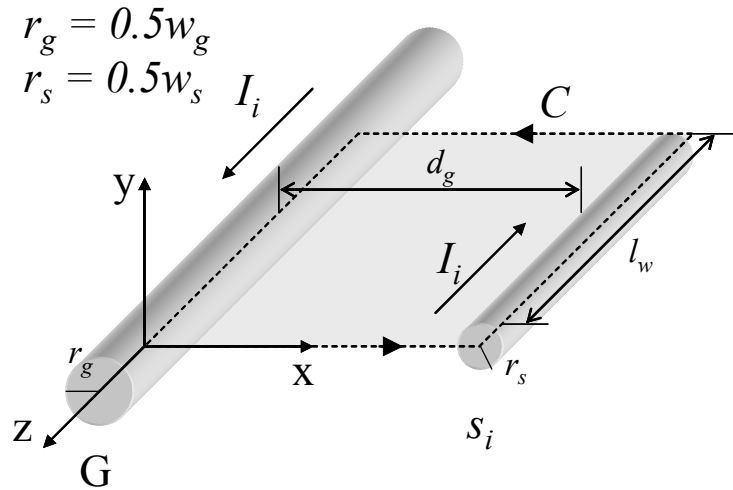


Figure 3: Degeneration of metal wire from Figure 2.

In the following discussion, we derive the magnetic flux density vector induced by a circular conductor which carrying current I_i . The cross-section view of the circular conductor is shown in Figure 4 where the radius of the conductor is b .

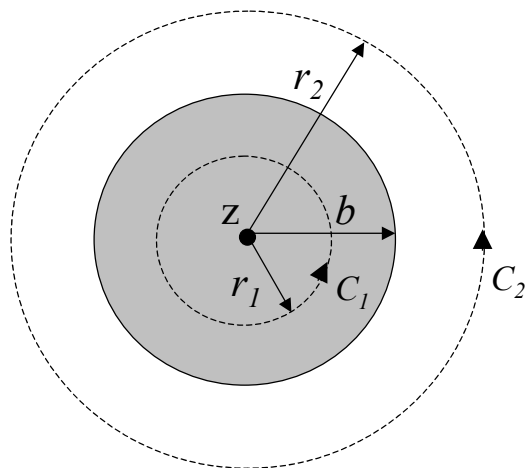


Figure 4: Cross-section view of a circular conductor with radius b .

If we align the conductor along the z-axis in the cylindrical coordinate, current I_i flows in z-direction, which is outward direction of this paper. Assumed that current I_i is uniformly distributed in the conductor and the conductor is infinitely long ($l_w \gg r$, r is the distance from the conductor's center to a certain point), we can derive Equations (8) and (9) using Equation (2).

$$\vec{B}_{in} = \hat{a}_\phi \frac{\mu_0 r_1 I_i}{2\pi b^2}, \quad r_1 \leq b \quad (8)$$

$$\vec{B}_{out} = \hat{a}_\phi \frac{\mu_0 I_i}{2\pi r_2}, \quad r_2 \geq b \quad (9)$$

where \vec{B}_{in} is the magnetic flux density vector inside the conductor and \vec{B}_{out} is the vector outside the conductor.

As N_i , S_i , and \vec{B}_i are already known, we can then derive the formula of the internal inductance per unit length, which is a part of the self-inductance, for a circular wire. Consider an annular ring in the inner conductor between radius r and $r + dr$ ($r \leq b$). The current in a unit length of this annular ring is linked by the flux that can be obtained by integrating Equation (8). We have

$$\begin{aligned} d\Phi'_{in} &= \int_r^b B_{in} dr \\ &= \frac{\mu_0 I_i}{4\pi b^2} (b^2 - r^2). \end{aligned} \quad (10)$$

The current in the annular ring, however, is only a fraction ($2\pi r dr / \pi b^2 = 2r dr / b^2$) of the total current I_i . As a result, the flux linkage for this annular ring is

$$d\Lambda'_{in} = \frac{2r dr}{b^2} d\Phi'. \quad (11)$$

Hence, we can obtain the total flux linkage per unit length by integrating Equation (11):

$$\begin{aligned} \Lambda'_{in} &= \int_0^b d\Lambda'_{in} \\ &= \frac{\mu_0 I_i}{8\pi}. \end{aligned} \quad (12)$$

The unit length internal inductance of the circular wire is

$$L'_{in} = \frac{\Lambda'_{in}}{I_i}$$

$$= \frac{\mu_0}{8\pi} \quad (13)$$

Then, the total internal self-inductance per unit length of the two wires system of Figure 3 is

$$\begin{aligned} L'_{in} &= 2 \times \frac{\mu_0}{8\pi} \\ &= \frac{\mu_0}{4\pi} \end{aligned} \quad (14)$$

After computing the internal self-inductance, we derive the external self-inductance. Now, We change the coordinate to the Cartesian coordinate. In the xz -plane where the two wires lie, as in Figure 3, the contributing \vec{B} vectors due to the equal and opposite currents in the two wires have only a y -component. Hence, from Equation (9), we obtain

$$B_G = \frac{\mu_0 I_i}{2\pi x} \quad (15)$$

and

$$B_{s_i} = \frac{\mu_0 I_i}{2\pi(d_g + r_g + r_s - x)} \quad (16)$$

The flux linkage per unit length is

$$\begin{aligned} \Phi'_{ex} &= \int_{r_g}^{r_g+d_g} (B_G + B_{s_i}) dx \\ &= \frac{\mu_0 I_i}{2\pi} \ln \left(\frac{(r_g + d_g)(r_s + d_g)}{r_s r_g} \right) \end{aligned} \quad (17)$$

Therefore, the unit length external inductance in Figure 3 is

$$\begin{aligned} L'_{ex} &= \frac{\Phi'_{ex}}{I_i} \\ &= \frac{\mu_0}{2\pi} \ln \left(\frac{(r_g + d_g)(r_s + d_g)}{r_s r_g} \right) \end{aligned} \quad (18)$$

Finally, we can obtain the total self-inductance (L_i) in Figure 3 by summing Equations (14) and (18) and then multiplying with the signal wire length l_w .

$$L_i = l_w (L'_{in} + L'_{ex})$$

$$= l_w \left(\frac{\mu_0}{4\pi} + \frac{\mu_0}{2\pi} \ln \left(\frac{(r_g + d_g)(r_s + d_g)}{r_s r_g} \right) \right) \quad (19)$$

If another ground wire exists on the other side of the signal wire separated by the distance d_{g2} ($d_{g2} \geq d_g$), the current flowing in the nearest G wire will decrease. We modify Equations (14) and (15) to Equations (20) and (21) with the branch current of $0.5I_i$, which is given from the *Kirchhoff's Current law* as follows:

$$L'_{in} = (1 + 0.5) \times \frac{\mu_0}{8\pi} \quad (20)$$

$$B_G = 0.5 \times \frac{\mu_0 I_i}{2\pi x} \quad (21)$$

Then, re-deriving Equations (17) to (19), the new self-inductance formula for the case when there are two ground wires can be obtained as follows:

$$L_i = l_w (L'_{in} + L'_{ex})$$

$$= \frac{l_w \mu_0}{2\pi} \left(0.375 + \ln \left(\frac{(r_g + d_g)^{0.5} (r_s + d_g)}{r_s r_g^{0.5}} \right) \right) \quad (22)$$

If there are n ground wires, we also simplify these cases to the two ground wires system. We named the above formula *AMAS* (Analytical Model Approximation of Self-inductance).

3.2 Coupling Inductance

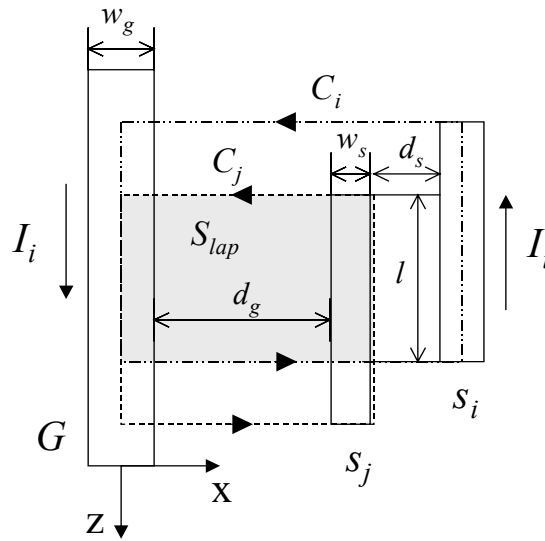


Figure 5: Top view of the coplanar structure.

As in the previous subsection, we first consider single ground wire system. The top view of the coplanar structure is shown in Figure 5. Now, we consider the xz -plane where the three wires lie, as shown in Figure 5. The contributing \vec{B} vectors due to the current flowing in G and s_i wire have only a y -component. From Equation (9), we have

$$B_G = \frac{\mu_0 I_i}{2\pi x} \quad (23)$$

and

$$B_{s_i} = \frac{\mu_0 I_i}{2\pi(0.5w_g + d_g + d_s + 1.5w_s - x)} \quad (24)$$

The coupling inductance L_{ij} is proportional to the overlapping area of S_i and S_j . The overlapping area S_{lap} is shown as the gray region in Figure 5. We can derive the flux linkage per unit length from Equation (4). We have

$$\begin{aligned} \Lambda'_{ex} &= \Phi'_{ex} \\ &= \frac{1}{l} \int_{S_{lap}} B ds_{lap} \\ &= \int_{0.5w_g}^{0.5w_g + d_g + w_s} (B_G + B_{s_i}) dx \\ &= \frac{\mu_0 I_i}{2\pi} \ln \left(\frac{(0.5w_g + d_g + w_s)(d_g + d_s + 1.5w_s)}{0.5w_g(d_s + 0.5w_s)} \right) \quad (25) \end{aligned}$$

Therefore, the external inductance is

$$L'_{ex} = \frac{\Lambda'_{ex}}{I_i} \quad (26)$$

and the internal inductance due to G wire is

$$L'_{in} = \frac{\mu_0}{8\pi} \quad (27)$$

Hence, the total coupling inductance of Figure 5 is

$$\begin{aligned} L_{ij} &= L_{ji} \\ &= l(L'_{in} + L'_{ex}) \end{aligned}$$

$$= \frac{l\mu_0}{2\pi} \left(\frac{1}{4} + \ln \left(\frac{(0.5w_g + d_g + w_s)(d_g + d_s + 1.5w_s)}{0.5w_g(d_s + 0.5w_s)} \right) \right). \quad (28)$$

If another ground wire exists on the other side of the signal wire with distance d_{g2} ($d_{g2} \geq d_g + d_s + w_s$), the current flowing in the nearest G wire will decrease. As in the previous subsection, we modify Equations (23) and (27) to Equations (29) and (30) with the branch current of $0.5I_i$:

$$B_G = 0.5 \times \frac{\mu_0 I_i}{2\pi x} \quad (29)$$

$$L'_{in} = 0.5 \times \frac{\mu_0}{8\pi}. \quad (30)$$

Re-deriving Equations (25), (26), and (28), the new coupling inductance formula for the case when there are two ground wires can be obtained as follows:

$$\begin{aligned} L_{ij} &= L_{ji} \\ &= l(L'_{in} + L'_{ex}) \\ &= \frac{l\mu_0}{2\pi} \left(\frac{1}{8} + \ln \left(\frac{(0.5w_g + d_g + w_s)^{0.5}(d_g + d_s + 1.5w_s)}{(0.5w_g)^{0.5}(d_s + 0.5w_s)} \right) \right). \quad (31) \end{aligned}$$

If there are n ground wires, we also simplify these cases to the two ground wires system as in Subsection 3.1. We named the above formula *AMAC* (Analytical Model Approximation of Coupling Inductance).

3.3 Modeling Short Wires and Small Coupling

Previous subsections are all based on the assumption that wires are sufficiently long, namely, $l_w \gg d_g$. When wire lengths are comparable to wire spaces, however, Equation (9) cannot be used to model the magnetic flux density, since we cannot find a closed path around the current-carrying wire such that the magnitude of \vec{B} is constant over the path. Besides, if two signal wires have no overlapping length between them, does the coupling inductance exist? The answer is affirmative, although the coupling inductance is very small. Therefore, if we use the equations derived in Subsections 3.1 and 3.2 for all cases of the coplanar structure, our approximations will cause a large amount of errors in some corner cases. Based on the above fact, we should use more sophisticated formulas to approximate the inductances for the situations, when

- (1) The wire length is comparable to its distance to the nearest ground wire.

(2) The overlapping length is much smaller than the signal wire length.

If above two situations are encountered, we should rederive the magnetic flux density vector induced from the wire before computing the inductance. In this subsection, we introduce the *Biot-Savart law*, Equation (32), to derive the formula of magnetic flux density vector.

$$\begin{aligned}\vec{B} &= \oint_{C'} d\vec{B} \\ &= \frac{\mu_0 I}{4\pi} \oint_{C'} \frac{d\vec{l}' \times \vec{R}}{R^3}\end{aligned}\quad (32)$$

where C' is the closed path of current I , and \vec{R} is the vector directed from the source to the field point. If we have a line segment carrying current I along the z -axis in the cylindrical coordinate shown in Figure 6.

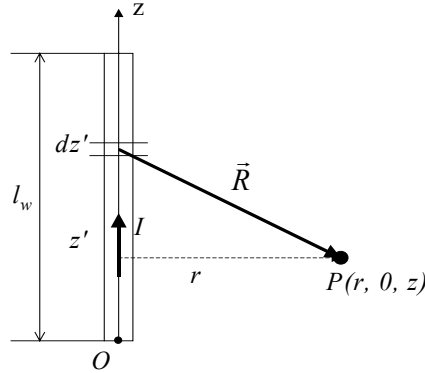


Figure 6: Top view of a carrying current wire.

Therefore,

$$\vec{R} = \hat{a}_r r + \hat{a}_z (z - z') \quad (33)$$

and

$$\begin{aligned}d\vec{l}' \times \vec{R} &= \hat{a}_z dz' \times (\hat{a}_r r + \hat{a}_z (z - z')) \\ &= \hat{a}_\phi r dz' .\end{aligned}\quad (34)$$

Using Equations (32) and (34), we can obtain

$$\vec{B} = \hat{a}_\phi \frac{\mu_0 I}{4\pi} \int_0^{l_w} \frac{rdz'}{(r^2 + (z - z')^2)^{3/2}}. \quad (35)$$

When the magnetic flux density vector is already known, we can then derive the formula of coupling inductance. Next, we consider the two ground wires system shown in Figure 7.

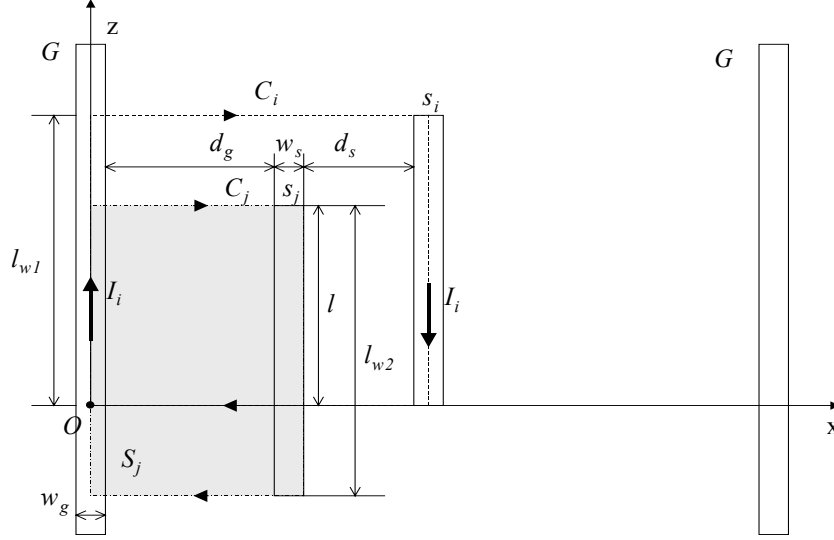


Figure 7: Top view of the coplanar structure.

The internal inductance is

$$L_{in} = 0.5 \times l \times \frac{\mu_0}{8\pi}. \quad (36)$$

From Equation (35), we know that the contributing \vec{B} vectors due to the equal and opposite currents in s_i and G wires have only a y -component in the Cartesian coordinate. Hence, the magnitude of the magnetic flux induced by the G wire of Figure 7 is

$$B_G = 0.5 \frac{\mu_0 I}{4\pi} \int_0^{l_w} \frac{xdz'}{(x^2 + (z - z')^2)^{3/2}}, \quad (37)$$

and the flux linkage due to the G wire is

$$\begin{aligned} \Lambda_G &= \Phi_G \\ &= \int_{S_j} B_G ds_j \end{aligned}$$

$$= \int_{0.5w_g}^{0.5w_g+d_g+w_s} \int_{l-l_w}^l B_G dz dx . \quad (38)$$

For the simplification of our formulation, we reverse the structure and align s_i with the z-axis as shown in Figure 8.

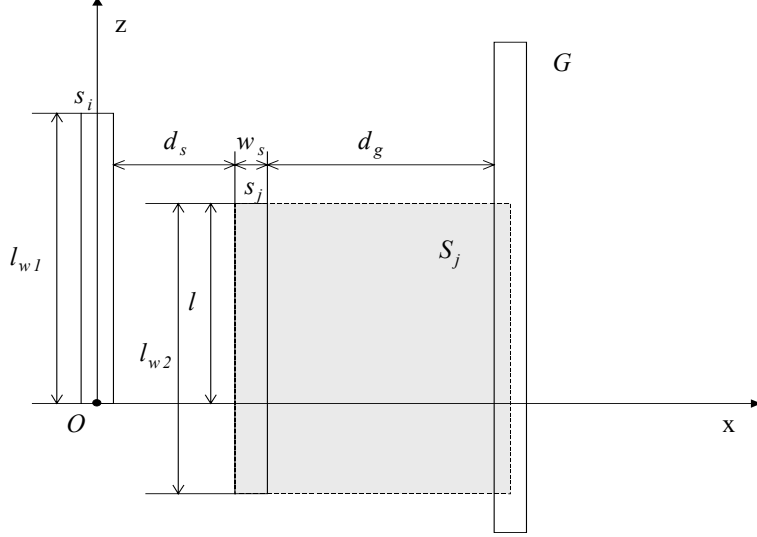


Figure 8: Reversed placement of Figure 7.

Then the magnitude of the magnetic flux induced by the s_i wire in Figure 8 is

$$B_{s_i} = \frac{\mu_0 I}{4\pi} \int_0^{l_w} \frac{x dz'}{(x^2 + (z - z')^2)^{3/2}} . \quad (39)$$

The flux linkage due to s_i wire is

$$\begin{aligned} \Lambda_{s_i} &= \Phi_{s_i} \\ &= \int_{S_j} B_{s_i} ds_j \\ &= \int_{0.5w_g}^{0.5w_g+d_g+w_s} \int_{l-l_w}^l B_{s_i} dz dx . \end{aligned} \quad (40)$$

Therefore, the total external inductance is

$$\begin{aligned} L_{ex} &= \frac{\Lambda_{ex}}{I_i} \\ &= \frac{(\Lambda_G + \Lambda_{s_i})}{I_i} . \end{aligned} \quad (41)$$

Hence, summing up Equations (36) and (41), we can compute the coupling inductance by

$$\begin{aligned} L_{ij} &= L_{in} + L_{ex} \\ &= 0.5l \frac{\mu_0}{8\pi} + L_{ex}. \end{aligned} \quad (42)$$

For the simplification of our equation, we do not expand the term L_{ex} . We named the above formula *IAMAC* (*I*mproved *A*nalytical *M*odel *A*pproximation of *C*oupling Inductance).

Next, we derive the formula of the self-inductance for the situation when a signal wire length is comparable to its distance to the nearest ground wire. We consider the coplanar structure shown in Figure 3 to derive the formula. The self-inductance also includes the internal and the external inductance. Therefore, in a two-ground wires system, the internal inductance is

$$L_{in} = (1 + 0.5) \times l_w \times \frac{\mu_0}{8\pi}. \quad (43)$$

Assume the loop area is S_j . Since $\Phi = \int_S \vec{B} \cdot d\vec{s}$, we have

$$\begin{aligned} \Lambda_G &= \Phi_G \\ &= \int_{S_j} B_G ds_j \\ &= \int_{0.5w_g}^{0.5w_g+d_g} \int_{l-l_w}^l B_G dzdx \end{aligned} \quad (44)$$

and

$$\begin{aligned} \Lambda_{s_i} &= \Phi_{s_i} \\ &= \int_{S_j} B_{s_i} ds_j \\ &= \int_{0.5w_s}^{0.5w_s+d_g} \int_{l-l_w}^l B_{s_i} dzdx. \end{aligned} \quad (45)$$

The formulae of B_G and B_{s_i} are the same as Equations (37) and (39). Then we obtain the total self-inductance (by Equations (41), (43), (44), and (45)) as follows

$$\begin{aligned} L_i &= L_{in} + L_{ex} \\ &= 1.5l_w \frac{\mu_0}{8\pi} + L_{ex}. \end{aligned} \quad (46)$$

Again, we do not expand the term L_{ex} for simplicity. We named the above formula *IAMAS* (*I*mproved *A*nalytical *M*odel *A*pproximation of *S*elf-inductance).

4. Experimental Results

We verify the accuracy of our formulae, *AMAS* (*A*nalytical *M*odel *A*pproximation of *S*elf-inductance), *AMAC* (*A*nalytical *M*odel *A*pproximation of *C*oupling Inductance), *IAMAC* (*I*mproved *A*nalytical *M*odel *A*pproximation of *C*oupling Inductance), and *IAMAS* (*I*mproved *A*nalytical *M*odel *A*pproximation of *S*elf-inductance), by comparing with FastHenry. In Subsection 4.1, experiments of various ground wire structures are conducted to find the applicable structures for our formulae. Subsection 4.2 verifies the accuracy of our formulae by using different parameters. We show that our formulae are also suitable for the bus structure in Subsection 4.3.

4.1 Ground Wire Structure

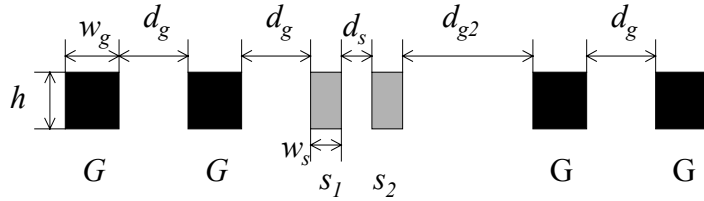


Figure 9: Cross-section view of the coplanar structure with multiple ground wires.

We discuss the effect of the number of ground wires on inductance in this subsection. Consider the cross-section view of the coplanar structure shown in Figure 9 for the first experiment. We represent the structure by GGs_1s_2GG . In our experiment, we set $h = 2\mu\text{m}$, $w_s = 0.8\mu\text{m}$, $d_s = 0.8\mu\text{m}$, $w_g = 2\mu\text{m}$, $d_g = 12\mu\text{m}$. Also, we set $d_{g2} = d_g + d_s + w_s = 18.4\mu\text{m}$ to make s_2 farther than s_1 to a nearest ground wire. The length of the G wire was $4500\mu\text{m}$, the lengths of both s_1 and s_2 were $l_w = 1000\mu\text{m}$, and the overlapping lengths of s_1 and s_2 were $l = 1000\mu\text{m}$. We experimented on the Gs_1s_2 , Gs_1s_2G , Gs_1s_2GG , Gs_1s_2GGG , GGs_1s_2 , $GGGs_1s_2$, $GGGGs_1s_2$, and GGs_1s_2GG structures and obtained the results shown in Figure 10, Figure 11, and Figure 12. From Figure 10, Figure 11, and Figure 12 we observe that our formulae are more suitable for the structures with two or more G wires since the results are closer to those obtained by FastHenry. This is a typical situation in a real design where there must be at least one ground and one power grids in a circuit.

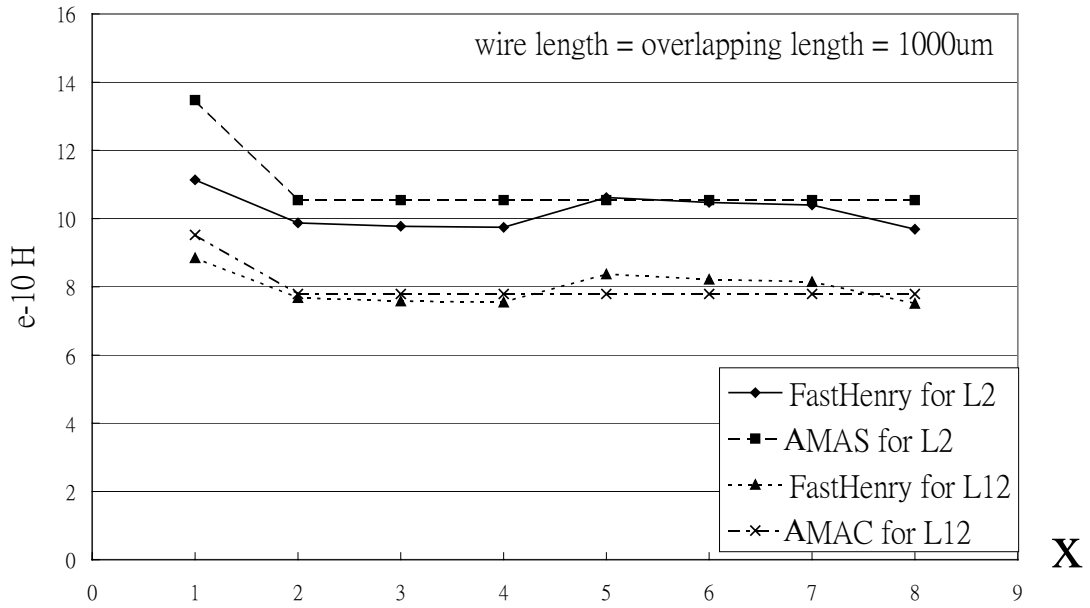


Figure 10: Experimental results for different coplanar structures, where x=1 stands for Gs_1s_2 , x=2 stands for Gs_1s_2G , x=3 stands for Gs_1s_2GG , x=4 stands for Gs_1s_2GGG , x=5 stands for GGs_1s_2 , x=6 stands for $GGGs_1s_2$, x=7 stands for $GGGGs_1s_2$, and x=8 stands for GGs_1s_2GG .

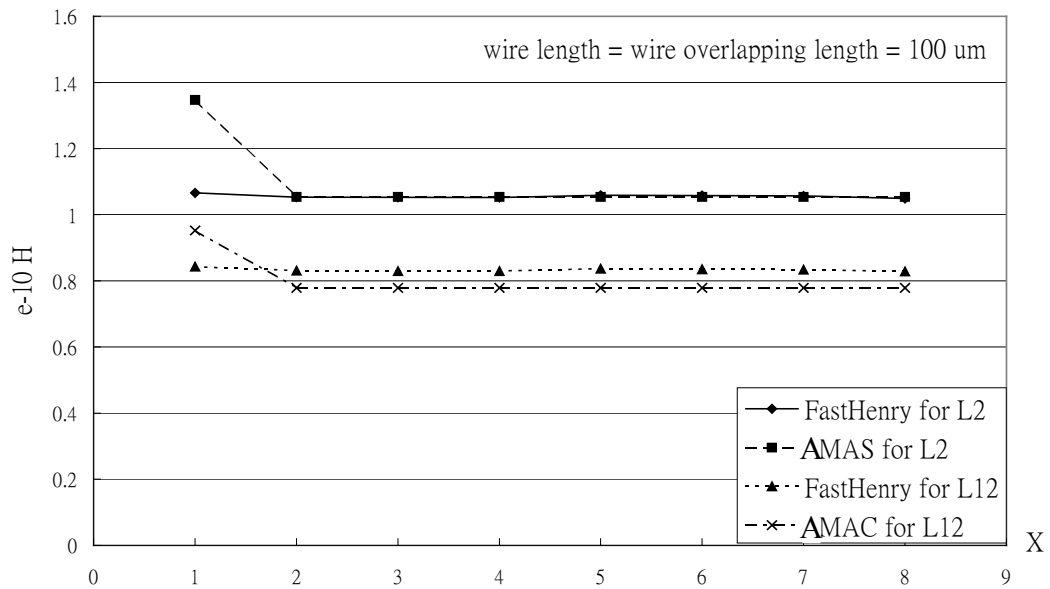


Figure 11: Experimental results for different coplanar structures, where x=1 stands for Gs_1s_2 , x=2 stands for Gs_1s_2G , x=3 stands for Gs_1s_2GG , x=4 stands for Gs_1s_2GGG , x=5 stands for GGs_1s_2 , x=6 stands for $GGGs_1s_2$, x=7 stands for $GGGGs_1s_2$, and x=8 stands for GGs_1s_2GG .

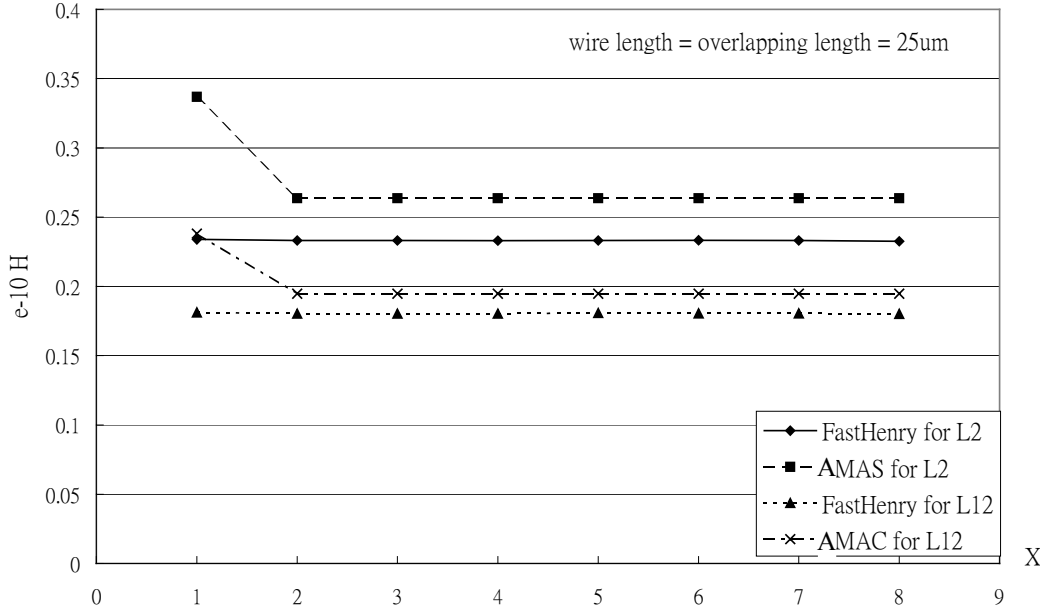


Figure 12: Experimental results for different coplanar structures, where $x=1$ stands for Gs_1s_2 , $x=2$ stands for Gs_1s_2G , $x=3$ stands for Gs_1s_2GG , $x=4$ stands for Gs_1s_2GGG , $x=5$ stands for GGs_1s_2 , $x=6$ stands for $GGGs_1s_2$, $x=7$ stands for $GGGGs_1s_2$, and $x=8$ stands for GGs_1s_2GG .

4.2 Accuracy of AMAS, AMAC, IAMAS, and IAMAC

In this subsection, we conducted the following two experiments: (1) the accuracy of *AMAS* and *IAMAS* for self-inductance extraction, and (2) accuracy of *AMAC* and *IAMAC* for coupling-inductance extraction. In the first experiment, we tested the accuracy of *AMAS* and *IAMAS* for self-inductance extraction in the Gs_1G structure with various l_w , d_g , w_s , w_g . The parameters, d_{g2} , d_g , h and the wire length of G wire, were identical to the previous experiments of previous subsection. The experimental results are given in Table 1. Identical values of parameters and conditions are applied to the third experiments on the coupling inductance whose results are shown in Table 2. Compared with FastHenry, the average errors of our modeling are within 10%, except the two corner cases: (1) the wire length is comparable to its distance to the nearest ground wire, and (2) the overlapping length is much smaller than the signal wire length. The errors may exceed 10% in these cases. This phenomenon proves our assumption in Subsection 3.3. For these corner cases, our improved formulae can achieve significantly more accurate estimations than the original ones, as shown in Table 1 and Table 2. In Figure 13 and Figure 14, the inductance values obtained by our modeling and FastHenry are plotted as functions of overlapping and wire lengths, respectively. The results show the accuracy of our work.

Self-inductance (Unit: 10^{-10} H)								
(l_w, d_g, w_s, w_g) (μm)	FastHenry	Time (sec)	<i>AMAS</i>	Time (sec)	Error (%)	<i>IAMAS</i>	Time (sec)	Error (%)
(2000, 12, 0.8, 2)	18.70280	117.09	20.3658	0.11	8.892	20.3299	8.02	8.700
(1500, 12, 0.8, 2)	14.51540	120.80	15.2744	0.11	5.229	15.2385	6.97	4.982
(1000, 12, 0.8, 2)	9.99291	103.41	10.1829	0.11	1.901	10.1470	5.82	1.542
(500, 12, 0.8, 2)	5.14302	106.79	5.0915	0.11	-1.003	5.0557	5.72	-1.698
(25, 12, 0.8, 2)	0.22642	99.75	0.2546	0.05	12.436	0.2232	6.15	-1.427
(10, 12, 0.8, 2)	0.07443	98.60	0.1018	0.06	36.806	0.0761	6.15	2.222
(1000, 12, 0.8, 4)	9.26282	111.57	9.3216	0.11	0.635	9.5280	5.66	2.863
(1000, 12, 0.8, 1)	10.59190	117.06	10.9551	0.11	3.429	10.8010	5.55	1.974
(1000, 12, 1.6, 2)	9.60097	110.11	8.8601	0.11	-7.716	8.8243	5.71	-8.090
(1000, 12, 0.4, 2)	10.24480	108.13	11.5367	0.11	12.610	11.5008	5.71	12.260
(1000, 24, 0.8, 2)	12.38490	99.46	12.1906	0.05	-1.569	12.1191	5.71	-2.146
(1000, 6, 0.8, 2)	7.73106	100.60	8.2411	0.05	6.597	8.2231	5.66	6.365
Average (absolute value)		107.78		0.09	8.235		6.07	4.522

Table 1: Experimental results of our modelings, *AMAS* and *IAMAS*, and FastHenry for self-inductances. The lengths of ground wires are $4,500\mu\text{m}$. We ran FastHenry on a SUN Ultra 60 model 1450 with dual CPUs and 2GB RAM and ran *AMAS* and *IAMAS* by using Mathematica Version 3.0 on a 566 MHz Celeron PC with 128 MB RAM.

Unit: μm		Coupling inductance (Unit: 10^{-10} H)							
Signal wire length	Overlapping length	FastHenry	Time (sec)	<i>AMAC</i>	Time (sec)	Error (%)	<i>IAMAC</i>	Time (sec)	Error (%)
2000	2000	17.1868	141.67	17.3525	0.11	0.964	17.2998	6.10	0.657
	1500	12.2176	141.98	13.0143	0.11	6.521	13.0140	15.82	6.518
1500	1500	13.4125	124.95	13.0143	0.11	-2.969	12.9617	7.19	-3.361
	1100	9.4542	120.45	9.5439	0.10	0.949	9.5434	16.98	0.944
	750	5.9326	125.98	6.5072	0.05	9.685	6.5071	4.94	9.683
1000	1000	9.2767	114.34	8.6762	0.06	-6.473	8.6237	5.66	-7.039
	750	6.8253	116.70	6.5072	0.05	-4.661	6.5064	15.70	-4.672
	500	4.3076	116.70	4.3381	0.05	0.709	4.3379	5.22	0.705
500	500	4.6593	110.60	4.3381	0.05	-6.894	4.2858	5.55	-8.016
	400	3.7163	110.28	3.4705	0.05	-6.614	3.4684	17.09	-6.669
	200	1.7031	110.00	1.7353	0.11	1.887	1.7352	9.12	1.884
100	50	0.4887	105.41	0.4338	0.11	-11.237	0.4321	4.94	-11.586
	25	0.2422	106.55	0.2169	0.06	-10.435	0.2191	11.70	-9.523
	5	0.0547	109.70	0.0434	0.05	-20.706	0.0561	12.03	2.553
Average (absolute value)			118.24		0.08	6.479		9.86	5.272

Table 2: Experimental results of our modelings, *AMAC* and *IAMAC*, and FastHenry for coupling inductances. Here, $w_s = d_s = 0.8\mu\text{m}$ for both signal wires, both ground wire length = $4,500\mu\text{m}$, $w_g = 2\mu\text{m}$, $d_g = 12\mu\text{m}$. We ran FastHenry on a SUN Ultra 60 model 1450 with dual CPUs and 2GB RAM and ran *AMAC* and *IAMAC* by using Mathematica Version 3.0 on a 566 MHz Celeron PC with 128 MB RAM.

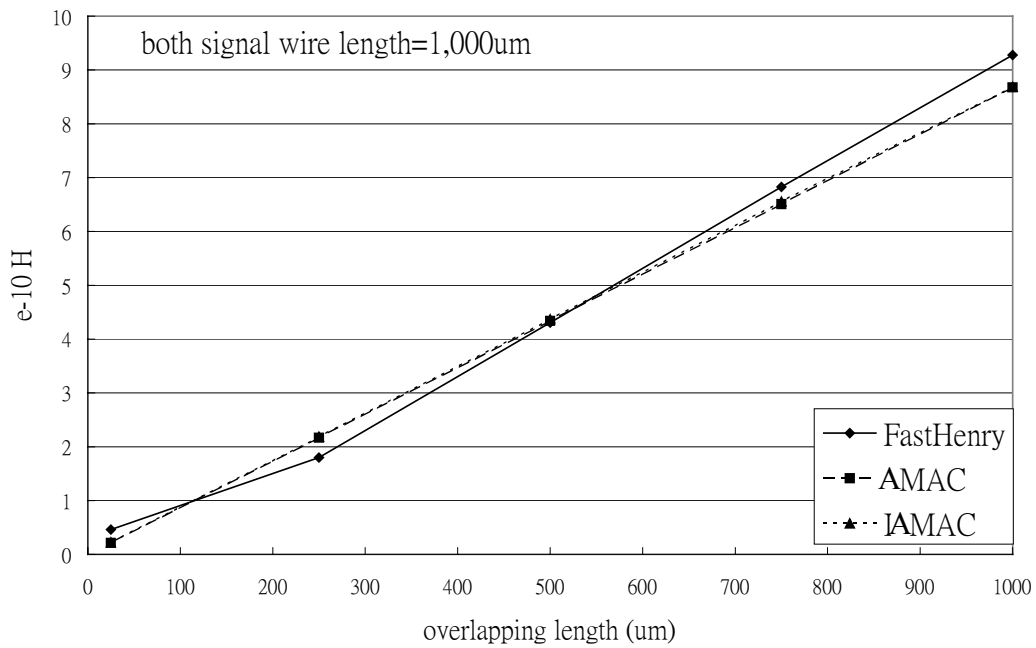


Figure 13: Coupling inductance vs. signal wire overlapping length when both signal wire length = 1,000 μ m, and the other parameters are identical to experiments in the previous subsection.

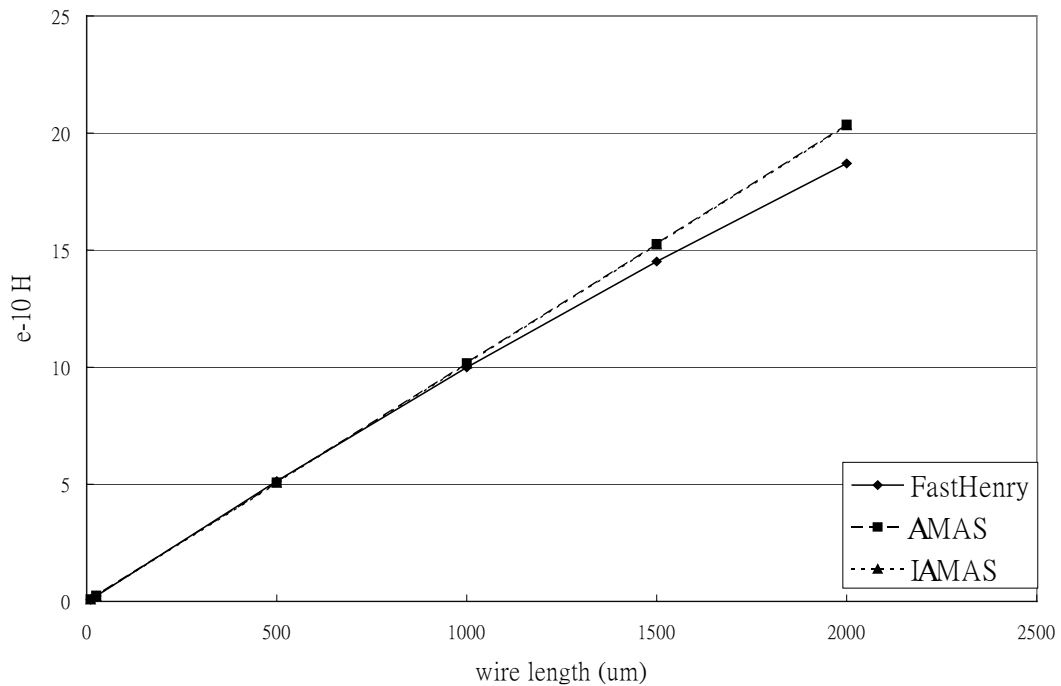


Figure 14: Self-inductance vs. signal wire length when the other parameters are identical to experiments in the previous subsection.

4.3 Experiments of Bus Structures

In this subsection, we experiment on the bus structure to show that our model is also suitable for the bus structure. In our experiment, the bus structure is 9-bit, all signal wire lengths are 2,000 μm , and the other parameters are the same as in the previous subsection. Table 3 lists the results.

Inductance (10^{-10} H)			
Routing	FastHenry	<i>AMAS&AMAC</i>	Error (%)
L_1	19.4186	20.3658	4.878
L_3	20.6165	21.7243	5.373
L_5	21.4648	22.8311	6.365
L_{13}	13.4016	12.6199	-5.833
L_{15}	11.1896	10.3177	-7.792
L_{35}	14.4393	13.7834	-4.542
Average error (absolute value)			5.797

Table 3: Self and mutual inductance estimated from FastHenry and our formulae for the bus structure (L_i stands the self-inductance of wire s_i ; L_{ij} stands the mutual inductance between wire s_i and s_j)

From Table 3, we can observe that the average difference between our simulation results and those obtained by FastHenry for the self and coupling inductance is about 5.8%. Therefore, our formulae are also suitable for the bus structure.

5. Conclusions

In this paper, we first introduced some basic electromagnetic concepts. Using these basic concepts, we derived analytical formulae to efficiently approximate the self and coupling inductance for wires of unequal lengths and dimensions. We first presented efficient formulae, *AMAS* and *AMAC*, for general cases. Then we derived more sophisticated formulae, *IAMAS* and *IAMAC*, for some corner cases to improve accuracy. By comparing with FastHenry, experimental results have shown the accuracy of our formulae. In particular, our modeling is extremely efficient, and thus can be incorporated into a layout tool for inductance optimization.

Reference

- [1] M. W. Beattie and L. T. Pileggi, "Inductance 101: Modeling and Extraction," *Design Automation Conference*, pp. 323–328, 2001.
- [2] M. W. Beattie, B. Krauter, L. Alatan, and L. Pileggi, "Equipotential Shells for Efficient Inductance Extraction," *IEEE Trans. Computer-Aided Design*, Vol. 20, Issue: 1, pp. 70–79, January 2001.
- [3] M. W. Beattie and L. T. Pileggi, "Electromagnetic Parasitic Extraction via a Multipole Method with Hierarchical Refinement," *International Conference on Computer Aided Design*, pp. 437–444, 1999.
- [4] C. K. Cheng, J. Lillis, S. Lin, and N. Chang, *Interconnect Analysis and Synthesis*, John Wiley and Sons Inc, 2000
- [5] D. K. Cheng, *Filed and Wave Electromagnetics*, 2nd Ed., Addison-Wesley, 1989.
- [6] L. Greengard, *The Rapid Evaluation of Potential Fields in Particle Systems*, The MIT Press, Cambridge, MA, 1987.
- [7] F. W. Grover, *Inductance Calculations: Working Formulas and Tables*, Dover Publications, New York, 1946.
- [8] L. He and K. M. Lepak, "Simultaneous Shield Insertion and Net Ordering for Capacitive and Inductive Coupling Minimization," *International Symposium on Physical Design*, pp. 55–60, 2000.
- [9] L. He, N. Chang, S. Lin, and O. S. Nakagawa, "An Efficient Inductance Modeling for On-chip Interconnects," *IEEE Custom Integrated Circuits Conference*, pp. 22.6.1–22.6.4, 1999.
- [10] Y. I. Ismail and E. G. Friedman, "Effects of Inductance on the Propagation Delay and Repeater Insertion in VLSI Circuits," *IEEE Trans. Very Large Scale Integration (VLSI) Systems*, Vol. 8, Issue: 2, April 2000.
- [11] M. Kamon, M. J. Tsuk, and J. K. White, "FastHenry: a Multipole-accelerated 3D Inductance Extraction Program," *IEEE Trans. Computer-Aided Design*, pp. 1750–1758, Sept. 1994
- [12] J. R. Phillips, M. Kamon, and J. White, "An FFT-based Approach to Including Non-deal Ground Planes in a Fast 3-D Inductance Extraction Program," *Proceedings of the IEEE Custom Integrated Circuits Conference*, pp. 8.3.1–8.3.4, 1993.
- [13] X. Qi, B. Kleveland, Z. Yu, S. Wong, R. Dutton, and T. Young, "On-Chip Inductance Modeling of VLSI Interconnects," *IEEE International Solid-State Circuits Conference*, pp. 172 -173, 2000.
- [14] Semiconductor Industry Association, *International Technology Roadmap for Semiconductors*, 1999.
- [15] G. Zhong, C. K. Koh, and K. Roy, "A Twisted-Bundle Layout Structure for Minimizing Inductive Coupling Noise," *IEEE International Conference on Computer Aided Design*, pp. 406–411, 2000.